XLIII CILAMCE
21–25, November, 2022
FOZ DO IGUAÇU – PR – BRAZIL

Numerical investigation on tornado-like flows and immersed bodies using vortex models

Miguel A. Aguirre[1], Alexandre L. Braun[1], Armando M. Awruch[1]

[1]*Centro de Mecânica Aplicada e Computacional (CEMACOM), Programa de Pós-Graduação em Engenharia Civil (PPGEC), Universidade Federal do Rio Grande do Sul (UFRGS)*
Avenida Osvaldo Aranha, 99, 90035-190, Rio Grande do Sul, Brazil
miguel.aguirre@ufrgs.br, alexandre.braun@ufrgs.br, amawruch@ufrgs.br

Abstract. A study on the characteristics of real and experimentally simulated tornado flows is carried out in this work using a numerical formulation based on the model of Vatistas et al. [1]. The flow governing equations are discretized using an explicit two-step Taylor-Galerkin scheme and a finite element formulation is used for spatial discretization, where eight-node hexahedral elements with reduced integration are used. Tornado flow fields are reproduced numerically from a velocity profile model by Vatistas et al. [1], where time-dependent boundary conditions are used to account for tornado vortex translation. Turbulence modeling is performed using Large Scale Simulation (LES) with the Smagorinsky sub-grid scale model and the computational code is parallelized using CUDA FORTRAN directives for processing on graphics cards. An experimentally generated tornado flow field is reproduced using the model implemented here and a cubic building model subjected to different tornado flow conditions is also analyzed. Results demonstrate that the velocity profile models are able to satisfactorily reproduce the tornado flow fields and the corresponding aerodynamic forces on immersed bodies.

Keywords: Computational Wind Engineering (CWE); Finite Element Method (FEM); Large Eddy Simulation (LES); Tornado flows; Vortex models.

1 Introduction

Tornadoes are natural phenomena occurring on every continent except in the Antarctic region, with higher incidence in some locations such as the central part of the United States of America, the southern region in Brazil, the northern zone in Argentina and the surrounding of Himalayas. Tornadoes generally present a localized and short-time action owing to its scale, which hinders its prediction and detailed analysis by radar measurements. In order to understand this phenomenon, in particular the flow configuration and interactions with immersed structures, some experimental simulators have been proposed in the last fifty years. More recently, with the development of numerical techniques and computer technology, numerical simulations have been also employed to reproduce the same flow characteristics found by experimental devices and field measurements.

Numerical models based on vortex velocity profiles take into account vortex motion and immersed bodies in a simple manner, although all the possible flow patterns observed in a tornado cannot be represented completely. Mathematical expressions for vortex models can be obtained by solving the Navier-Stokes equations in cylindrical coordinates for particular situations. The Rankine Combined Vortex Model (RCVM), for instance, is deduced by considering an ideal fluid with a velocity field composed of two regions: the forced vortex region in the inner core and the external free vortex region, where only the tangential velocity is not null. In the Burgers-Rott Model, the three velocity components and pressure are considered to form a unicellular vortex. A similar approach is also considered in the Sullivan Model, but forming a two-cell vortex. In recent years, algebraic velocity profiles have been developed, which try to approximate all these models simultaneously using a single model. Strasser and Selvam [2] used the Algebraic Model proposed by Vatistas et al. [1] to simulate the vortex-cylinder interaction in a two-dimensional model by varying their relative size and the impact time. A

detailed comparison of vortex velocity models may be found in Strasser and Selvam [3].

A numerical investigation considering tornado models based on velocity profiles is performed in this work in order to evaluate typical tornado flow fields and aerodynamic loads produced by tornado flows on immersed bodies. The numerical model adopted in this paper is built using the explicit two-step Taylor-Galerkin scheme in the context of the Finite Element Method (FEM), where hexahedral elements with one-point integration and hourglass control are utilized for spatial discretization. Turbulence is considered using Large Eddy Simulation (LES) and Smagorinsky's sub-grid scale model. The flow is supposed to be incompressible, although the pseudo-compressibility hypothesis is adopted, and an isothermal process is assumed. Tornado flow fields generated experimentally are reproduced using the vortex model proposed here.

2 Numerical model

In the field of Computational Wind Engineering (CWE), wind flows are generally assumed to be incompressible, turbulent and isothermal, where the air is considered as a Newtonian fluid with no gravity effects (see [4]). In this work, an Eulerian formulation is adopted for the kinematic description of the flow field using a Cartesian coordinate system and Large Eddy Simulation (LES) is utilized to simulate turbulent flows.

The flow numerical analysis is performed here using the explicit two-step Taylor-Galerkin scheme in the context of the Finite Element Method, where eight-node hexahedral elements with one-point quadrature and hourglass control are utilized in order to avoid spurious modes. The weak form of the finite element equations are finally obtained applying the Bubnov-Galerkin weighted residual method and the Green-Gauss theorem on the flow fundamental equations, which leads to the following system of matrix equations:

$$\overline{\mathbf{v}}_i^{n+1/2} = \mathbf{v}_i^n - \mathbf{M}_D^{-1}\frac{\Delta t}{2}\left[\left(\mathbf{A}+\mathbf{B}\right)\mathbf{v}_i^n + \mathbf{D}_{ij}\mathbf{v}_j^n - \mathbf{G}_i^{\mathrm{T}}\mathbf{p}^n - \mathbf{t}_i^n\right] \tag{1}$$

$$\mathbf{p}^{n+1/2} = \mathbf{M}_D^{-1}\mathbf{M}^*\mathbf{p}^n - \mathbf{M}_D^{-1}\frac{\Delta t}{2}\left(\rho c^2\mathbf{G}_j\mathbf{v}_j^n\right) \tag{2}$$

$$\mathbf{v}_i^{n+1/2} = \overline{\mathbf{v}}_i^{n+1/2} - \frac{\Delta t}{4\rho}\mathbf{M}_D^{-1}\mathbf{G}_i^{\mathrm{T}}\left(\mathbf{p}^{n+1/2} - \mathbf{p}^n\right) \tag{3}$$

$$\mathbf{v}_i^{n+1} = \mathbf{v}_i^n - \mathbf{M}_D^{-1}\Delta t\left(\mathbf{A}\mathbf{v}_i^{n+1/2} + \mathbf{D}_{ij}\mathbf{v}_j^{n+1/2} - \mathbf{G}_i^{\mathrm{T}}\mathbf{p}^{n+1/2} - \mathbf{t}_i^{n+1/2}\right) \tag{4}$$

$$\mathbf{p}^{n+1} = \mathbf{M}_D^{-1}\mathbf{M}^*\mathbf{p}^n - \mathbf{M}_D^{-1}\Delta t\left(\rho c^2\mathbf{G}_j\mathbf{v}_j^{n+1/2}\right) \tag{5}$$

where $\mathbf{p}$ and $\mathbf{v}_i$ are the finite element vectors containing pressure and velocity components (i = 1, 2, 3) evaluated at element nodes. The element matrices $\mathbf{M}_D$ and $\mathbf{M}^*$ are the lumped mass matrix and the modified mass matrix is utilized to stabilize the pressure field, which is given by $\mathbf{M}^* = e\mathbf{M}_D + (1 - e)\mathbf{M}$, where $\mathbf{M}$ is the consistent mass matrix and e is a selective lumping parameter ($0 \le e \le 1$). The remaining element matrices and vectors are defined as follows: $\mathbf{A}$ and $\mathbf{B}$ are the advection and stabilization matrices, $\mathbf{D}_{ij}$ are the diffusion matrices, $\mathbf{G}_i$ are the gradient matrices and $\mathbf{t}_i$ are the traction vectors referring to the boundary terms (i, j = 1, 2, 3). Hexahedral elements with trilinear interpolation functions are employed here for approximation of both, the velocity and pressure fields. By using one-point integration, the finite element matrices and vectors can be evaluated analytically. However, an hourglass control numerical technique to avoid spurious modes on diffusive terms must be utilized. Additional details on the finite element formulation employed in this work may be found in Braun and Awruch [4], [5].

2.1 Boundary conditions for tornado flow generations

According to Strasser and Selvam [3], the cross-section of a tornado vortex may be considered as a composition of three different regions (see Fig. 1a): (1) internal laminar core, (2) transition region and (3) external turbulent region, where the flow velocity field may be decomposed into translation and tangential velocity components. Figure 1 shows some typical tangential velocity profiles utilized by different authors,

which indicates that the tangential velocity values (V_θ) increase with the distance r to the vortex center, where a maximum value is obtained ($V_{\theta,max}$) at the critical radius r_c. For $r > r_c$ the tangential velocity values decrease as the distance to the vortex center is increased.

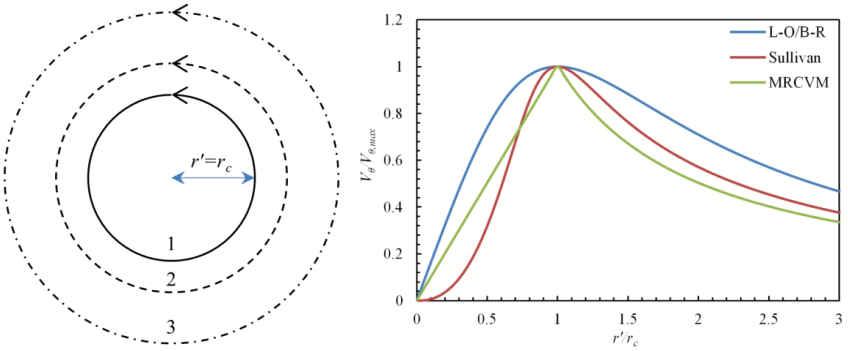

(a) (b)

Figure 1 – Analytical models for the tangential velocity profile: (a) schematic view of the vortex regions; (b) distribution of the normalized tangential velocity ($V_\theta / V_{\theta,max}$) over the relative radius (r'/r_c).

In the present work, the tangential velocity profile corresponding to the Vatistas Model – VM [1] is utilized as follows:

$$V_\theta^{VM}\left(r'\right) = \omega \cdot r' \cdot r_c^{\,2} \cdot \left(\frac{2}{\left(r'^{2\beta} + r_c^{\,2\beta} \right)} \right)^{1/\beta} \tag{6}$$

where the Lamb-Oseen/Burgers-Rott (L-O/B-R) tangential velocity profile is obtained when $\beta = 2$, and the RCVM model for $\beta = 100$. The maximum tangential velocity is obtained at r_c, where $V_{\theta,max}\left(r_c\right) = \omega r_c$, being ω the vortex angular velocity. In addition, the Vatistas model is able to derive two additional velocity components using the tangential component and the flow equations of motion, which may be written as:

$$V_r^{VM}\left(r'\right) = -2\left(\beta+1\right)\left(\frac{\nu_e}{r_c}\right)\frac{\left(\dfrac{r'}{r_c}\right)^{2\beta-1}}{1+\left(\dfrac{r'}{r_c}\right)^{2\beta}} \tag{7}$$

$$V_z^{VM}\left(r'\right) = 4\beta\left(\beta+1\right)\left(\frac{\nu_e}{r_c}\right)\left(\frac{z}{r_c}\right)\frac{\left(\dfrac{r'}{r_c}\right)^{2(\beta-1)}}{\left[1+\left(\dfrac{r'}{r_c}\right)^{2\beta}\right]^2} \tag{8}$$

where ν_e is the turbulent viscosity, with usual values of eddy viscosity specified in a range from 1 m^2/s to 10 m^2/s. The radial and vertical velocities are relatively small when they are compared with the tangential component, where the radial velocity component is usually the smallest. One can see that the radial velocity component shows negative values and the flow field is directed to the tornado center (radial inflow), while the vertical velocity component increases with height.

3 Numerical applications

3.1 Tornado-like vortex simulation

A stationary tornado flow field generated experimentally is obtained in this first application using the numerical model proposed in this work with the Vatistas vortex model. The experimental work is based on the ISU-type tornado-like-vortex simulator utilized by Wang et al. [6], which was also reproduced later by Cao et al. [7] using numerical techniques. Figure 2 shows the computational domain and boundary conditions utilized here, where the finite element mesh is constituted by 3,047,499 hexahedral elements and 3,078,688 nodes, with the smallest element length observed next to the ground at the axis of the cylindrical grid, with a characteristic length equal to 0.001 m. In order to simulate the tornado flow, velocity boundary conditions are considered on the top and lateral walls of the computational domain, where all the three velocity components are imposed, while null pressure is considered only on the lateral walls. The non-slip condition is adopted on the ground surface.

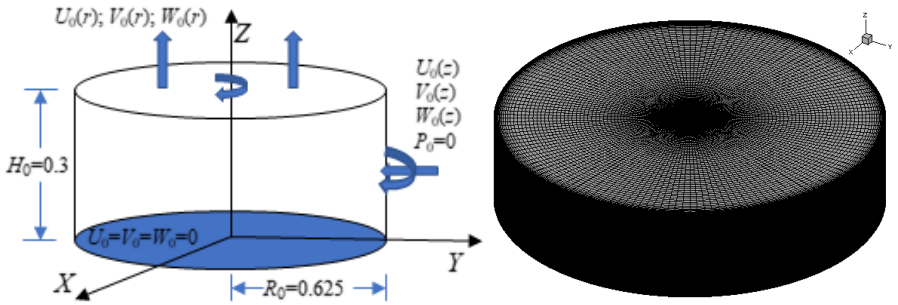

(a) (b)

Figure 2 – Tornado-like vortex simulation: a) computational domain and boundary conditions; b) computational mesh.

Table 1 – Numerical parameters adopted in the tornado vortex simulation.

Parameter	Combination 1	Combination 2	Combination 3
Swirl ratio – S	0.72 (S_{tan})	0.72 (S_{tan})	0.72 (S_{cir})
Eddy viscosity – Vatistas model parameter - ν_e	0.507 m^2/s	1.326 m^2/s	1.300 m^2/s
Vatistas parameter - β	2.0	2.0	2.0
Tornado critical radius – r_c	0.406 m	0.558 m	0.406 m
Tornado center coordinates – (x,y)	(0;0) m	(0;0) m	(0;0) m
Angular velocity – ω	7.992 rad/s	6.146 rad/s	7.992 rad/s
Reference velocity - U_∞	4.589 m/s	4.850 m/s	4.589 m/s

Table 2 – Parameters defining the tornado flow structure.

Parameters	Comb. 1	Comb. 2	Comb. 3	Wang et al. [6]	Cao et al. [7]
Max. tang. vel. – $V_{\theta,max}$	13.085 m/s	14.035 m/s	11.098 m/s	13.5 m/s	5.378 m/s
Radius at $V_{\theta,max}$ – R_{max}	0.079 m	0.086 m	0.143 m	0.067 m	0.058 m
Height at $V_{\theta,max}$ – h_{max}	0.017 m	0.014 m	0.136 m	0.015 m	0.021 m
Max. tang. vel. at h = 50 mm – $V_{\theta,max,h}$	10.515 m/s	12.629 m/s	9.837 m/s	11 m/s	4.263 m/s
Radius at $V_{\theta,max,h}$ – $R_{max,h}$	0.156 m	0.156 m	0.146 m	0.083 m	0.096 m
Radial Reynolds number – Re_r	$8.973x10^3$	$1.000x10^4$	$1.561x10^4$	$9.1x10^3$ - $1.4x10^4$	$1.22x10^5$*

*$Re = Q/H\nu$.

Tornado flow characteristics are defined here considering the swirl ratio S and Reynolds number Re as indicated in Table 1, where numerical parameters corresponding to three combinations are utilized here to reproduce the experimental tornado flow field. Numerical constants utilized in the present simulations are defined as follows: pseudo-compressibility parameter – c = 22.944 m/s (combinations 1 and 3) and 24.250 m/s (combination 2); selective lumping parameter – e = 0.9; Smagorinsky's constant – C_S = 0.1; time increment – Δt = 1.047x10^{-5} s (combinations 1 and 3) and 9.904x10^{-6} s (combination 2). The swirl ratio is calculated considering the following expression: $S_{tan} = \tan\theta/2a$, where θ is the orientation angle of guide vanes and $a = H/r_0$ is the aspect ratio (with H as the inflow height and r_0 as the radius of the updraft hole), both associated with the geometric characteristics of the experimental simulator (see [6], [7]). The swirl ratio may be also expressed as $S_{cir} = \Gamma/2Qa$, where Q is the volume flow rate calculated at the outflow boundary considering the vertical component of the flow velocity, and Γ is the free-stream circulation, which is evaluated at the outer edge of the convergence region using the following expression: $\Gamma = 2\pi R \int_0^H V_t dz$, where R is the radius of the convergence region and V_t is the mean tangential velocity evaluated locally.

Preliminary results obtained with the present model are compared (see Table 2) with experimental predictions presented by Wang et al. [6] and numerical results obtained by Cao et al. [7]. One can see that the sets of numerical parameters related to Combination 1 and Combination 2 lead to results similar to those obtained experimentally by Wang et al. [6].

Figure 3 presents pressure and velocity results corresponding to time-averaged fields obtained with the present formulation by adopting the numerical parameters corresponding to Combination 2, where the velocity fields correspond to the tangential component. One can observe the velocity field shows a distribution with maximum values observed in a region near the tornado center, where the velocity magnitude increases with the radial distance from the vortex center, and decreases for radial distances beyond the core radius. The pressure field presents usually high suction along the tornado axis with a typical funnel-shaped distribution.

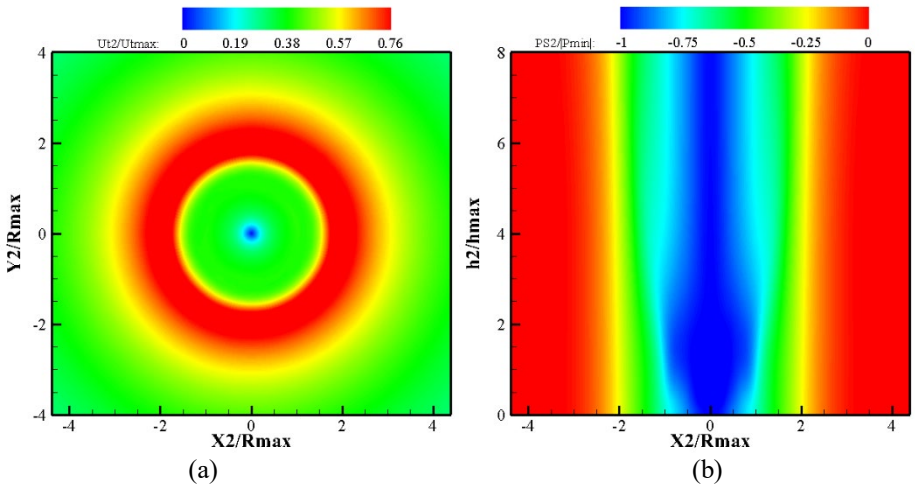

Figure 3 – Tornado vortex simulation: (a) time-averaged tangential velocity; (b) time-averaged pressure field.

Some tornado characteristics are evaluated comparatively in Fig. 4, where time-averaged profiles of pressure and velocity components are shown considering numerical, experimental and field data. Horizontal profiles of tangential velocity (Fig. 4a) are evaluated at a height corresponding to the ratio h/R_{max} = 0.5, with experimental data obtained by Wang et al. [6] and Cao et al. [7] and field measurement data referring to the Spencer tornado. The tangential velocity component and radial distance to tornado vortex center are normalized using the maximum tangential speed $U_{tmax,h}$ (= $V_{\theta,max,h}$, see Table 5) obtained at height h = 50 mm and the respective vortex radius. One can see that the tangential velocity profiles show similar results and a typical distribution, where the velocity values increase up to the maximum value obtained at the vortex core radius and decrease for radial distances outside the vortex core. On the other hand, all the parameter combinations tested here presented velocity values below the reference values utilized in the present investigation.

Pressure distribution along the radial direction (Fig. 4b) is obtained here at a height corresponding to the ratio h/R_{max} = 1, which is compared with experimental predictions obtained by Wang et al. [6], numerical results

obtained by Cao et al. [7] and field measurements referring to the Tipton tornado. Pressure values and radial distance are normalized considering the absolute maximum mean pressure drop P_{min} and the radial position where half of the time-averaged maximum pressure is observed ($r_{0.5Pmin}$). Results predicted with the present numerical model show a good agreement with experimental and field data. One can see that a significant pressure drop is identified around the centre of the tornado vortex, which is explained by the upward motion observed in that region. In addition, it is important to notice that pressure values vary significantly with height only for regions near the ground.

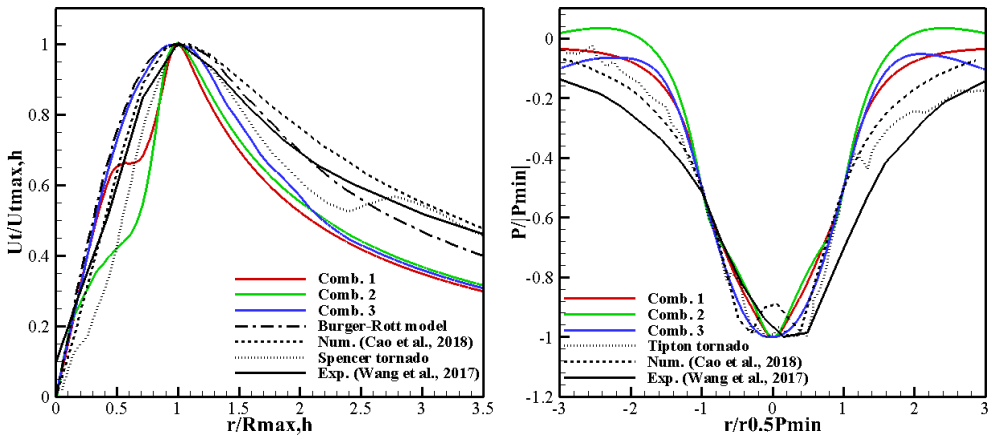

Figure 4 – Tornado vortex, time-averaged characteristics: (a) tangential velocity, horizontal profile; (b) pressure, horizontal profile.

3.2 Cubic building model subject to stationary tornado

Aerodynamic forces are evaluated in the present application considering a cubic building model (50mm x 50mm x 50mm) subject to stationary tornado-like vortex flow. The same flow characteristics and the same computational domain adopted in the previous example are utilized here (see Fig. 5a).

Figure 5b presents a time-averaged distribution of pressure coefficient on the building walls is shown. Results presented here correspond to predictions obtained using the set of parameters referring to Combination 2. In general, the pressure coefficient values predicted from the present simulation are approximately 10-15% greater than those presented by the reference work, where the maximum pressure coefficient obtained here is C_p = -1.650, while Cao et al. [7] obtained C_p = -1.405.

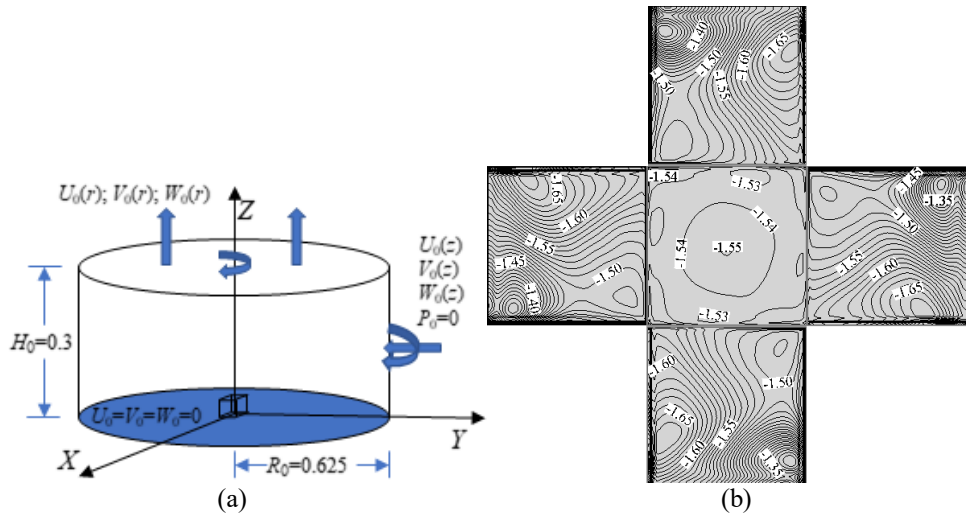

Figure 5 – Cubic building subjected to a stationary tornado flow: (a) computational domain and boundary conditions; (b) time-averaged pressure coefficient on the building walls.

Time-averaged results corresponding to aerodynamic force coefficients induced by the tornado flow on the building model are summarized in Table 6, where experimental predictions obtained by Wang et al. [8] and numerical results obtained by Liu and Ishihara [9] and Cao et al. [7] are also presented. It is observed that the numerical predictions obtained with the present formulation show high time-averaged forces along the lift component when the tornado center is located on the building top, while the time-averaged radial and tangential force components show insignificant values. Although Liu and Ishihara [9] and Wang et al. [8] present similar profiles for the tangential velocity component, some flow aspects are different, leading to different wind loads. In addition, Cao et al. [7] suggested that these deviations are possibly due to low measurement accuracy, which is induced on the experimental predictions by vortex wander. In addition, it is important to notice that Wang et al. [8] utilized a cubic model presenting small leakage holes with 0.05% opening ratio.

Table 6 – Cubic building subjected to a stationary tornado flow, time-averaged force coefficients.

Reference	Fr	Ft	Fv
Present work (Comb. 2)	-0.003	-0.003	2.056
Wang et al. [8] – Exp.	-0.327	-0.139	0.904
Liu and Ishihara [9] – Num.	0.000	0.027	1.918
Cao et al. [7] – Num.	-0.064	0.018	1.427

4 Conclusions

A numerical investigation to evaluate tornado flows and interactions with immersed body was proposed in the present work, where a finite element formulation based on vortex profile models was utilized. Flow fields induced by tornado-like vortices were generated here considering time-dependent boundary conditions imposed on the computational domain according to the Vatistas models, while LES was adopted to model turbulent flows. A stationary tornado flow field generated experimentally was reproduced with the numerical formulation proposed in this work. Results obtained here showed a good agreement with experimental, numerical and field data presented by other authors. It was observed that vortex models can reproduce experimental tornado flows and wind-induced loads on immersed bodies satisfactorily, since boundary conditions and vortex model parameters are calibrated properly.

Acknowledgements. The authors would like to thank the National Council for Scientific and Technological Development (CNPq, Brazil) and Brazilian Federal Agency for Support and Evaluation of Graduate Education (CAPES, Brazil) for the financial support. The present research was developed using computational resources provided by the National Center for Supercomputing (CESUP/UFRGS, Brazil), High Performance Computing Center (NACAD/UFRJ, Brazil) and National Center for High Performance Computing (CENAPAD/UNICAMP, Brazil).

Authorship statement. The authors hereby confirm that they are the sole liable persons responsible for the authorship of this work, and that all material that has been herein included as part of the present paper is either the property (and authorship) of the authors, or has the permission of the owners to be included here.

References

[1] G. H. Vatistas, V. Kozel, and W. C. Mih, "A simpler model for concentrated vortices," *Exp. Fluids*, vol. 11, no. 1, pp. 73–76, Apr. 1991, doi: 10.1007/BF00198434.

[2] M. N. Strasser and R. P. Selvam, "The variation in the maximum loading of a circular cylinder impacted by a 2D vortex with time of impact," *J. Fluids Struct.*, vol. 58, pp. 66–78, 2015, doi: 10.1016/j.jfluidstructs.2015.07.005.

[3] M. N. Strasser and R. P. Selvam, "Selection of a Realistic Viscous Vortex Tangential Velocity Profile for Computer Simulation of Vortex-Structure Interaction," *J. Ark. Acad. Sci.*, vol. 69, pp. 88–97, 2015.

[4] A. L. Braun and A. M. Awruch, "Aerodynamic and aeroelastic analyses on the CAARC standard tall building model using numerical simulation," *Comput. Struct.*, vol. 87, no. 9–10, pp. 564–581, 2009, doi: 10.1016/j.compstruc.2009.02.002.

[5] A. L. Braun and A. M. Awruch, "Finite element simulation of the wind action over bridge sectional models:

Application to the Guamá River Bridge (Pará State, Brazil)," *Finite Elem. Anal. Des.*, vol. 44, pp. 105–122, 2008, doi: 10.1016/j.finel.2007.11.006.

[6] J. Wang, S. Cao, W. Pang, and J. Cao, "Experimental Study on Effects of Ground Roughness on Flow Characteristics of Tornado-Like Vortices," *Boundary-Layer Meteorol.*, vol. 162, no. 2, pp. 319–339, 2017, doi: 10.1007/s10546-016-0201-6.

[7] S. Cao, M. Wang, and J. Cao, "Numerical study of wind pressure on low-rise buildings induced by tornado-like flows," *J. Wind Eng. Ind. Aerodyn.*, vol. 183, pp. 214–222, 2018, doi: 10.1016/j.jweia.2018.10.023.

[8] J. Wang, S. Cao, W. Pang, and J. Cao, "Experimental Study on Tornado-Induced Wind Pressures on a Cubic Building with Openings," *J. Struct. Eng.*, vol. 144, no. 2, 2018, doi: 10.1061/(asce)st.1943-541x.0001952.

[9] Z. Liu and T. Ishihara, "A study of tornado induced mean aerodynamic forces on a gable-roofed building by the large eddy simulations," *J. Wind Eng. Ind. Aerodyn.*, vol. 146, pp. 39–50, 2015, doi: 10.1016/j.jweia.2015.08.002.